Performance Analysis of a Tactile Sensor

David M. Siegel, Steven M. Drucker, Iñaki Garabieta
The MIT Artificial Intelligence Laboratory
545 Technology Square
Cambridge, MA 02139

Introduction

This paper discusses the design of a contact sensor for use with the Utah-MIT dexterous hand [Jacobsen, et al. 1984]. The sensor utilizes an 8×8 array of capacitive cells. This paper extends the work presented in Siegel and Garabieta [1986], and the earlier work of Boie [1984]; a more detailed design analysis, modifications to the construction process, and better performance results, are shown.

Design Issues

Many tactile sensor designs have been reported in the literature and a few have recently been made into commercial products [Dario and De Rossi 1985; Ogorek 1985; Harmon 1982]. However, none of the reported sensors meet the previously described requirements for the Utah-MIT hand. Problems with packaging, reliability, size, and sensitivity preclude their use.

The most common technologies employed by tactile sensors are based on optics, resistance, magnetics, and capacitance. All sensors, regardless of their underlying transduction principle, must convert an applied force into a measurable electric signal. The approach selected for our sensor is based on measuring the capacitance between two surfaces separated by a compressive material.

Two parallel electrically conductive plates generate a capacitance proportional to their separation. If a compressible dielectric is placed between them, a force applied to the capacitor's top surface will reduce the plate separation distance. The resulting change in capacitance can be used to infer the applied force. This principle is the basis of the capacitive tactile sensor's force transduction mechanism.

An array of capacitive cells is formed by sandwiching a dielectric layer between two sets of parallel conducting traces, with the top etches perpendicular to the bottom ones. A capacitor is formed each time an upper trace intersects a lower trace. To make an array of 64 force sensing capacitors, 8 upper traces and 8 lower traces are used.

As previously mentioned, the basic operating principle for the tactile sensors is the measurement of an applied pressure by detecting a variation in the gap of two parallel capacitive plates. Hence, the material between the two plates is a crucial component of the device; it forms both the elastic layer that compresses in response to pressure, and the dielectric layer that provides the capacitance between the two plates.

Ideally, this material should compress linearly as force on it increases. This spring-like behavior is given by

$$F = k\Delta X, \tag{1}$$

where F is the applied force, k is the effective spring constant, and ΔX is the positional change that the force produces. Having a material that closely approximates this equation makes it easy to translate the output of the sensor back to the applied force, since the detected capacitance will then vary in linear correspondence to the force. Thus, the material selected should have linear compression over the range of pressures to be applied.

The dielectric layer is composed of an electrically insulating silicone rubber. Silicone rubber has the desirable flexibility and durability that the layer requires. In addition, its dielectric constant is approximately 4, which increases the overall performance of the device by increasing each cell's effective capacitance.

Although the silicon rubber is flexible, it does not have desirable continuum mechanical properties. In fact, it is largely incompressible when subjected to a uniform pressure applied over its surface. Since the tactile sensor detects an applied stimulus by measuring the resulting deformation profile that it generates, a solid object pushing uniformly into the pad will not excite a response.

To better understand the behavior of the rubber medium, consider it to be composed of small unit volume cubes with xyz coordinate frames. Assume that the yz plane is aligned with the material's surface, and forces are applied along the x axis. Stresses are related to strains by Hooke's law, where E is the modulus of elasticity.

For the small cube, Timoshenko and Goodier [1951] gives the relationship between stresses and strains as

$$\begin{aligned} \epsilon_x &= \frac{1}{E}\left(\sigma_x - \tfrac{1}{2}(\sigma_y + \sigma_z)\right) \\ \epsilon_y &= \frac{1}{E}\left(\sigma_y - \tfrac{1}{2}(\sigma_x + \sigma_z)\right) \\ \epsilon_z &= \frac{1}{E}\left(\sigma_z - \tfrac{1}{2}(\sigma_x + \sigma_y)\right) \end{aligned} \tag{2}$$

where σ is the applied stress and ϵ is the resulting strain. Assuming the sensor uses a flat rubber sheet with its bottom glued to a rigid mounting surface, the y and z axis of the cube undergo hardly any positional change when a uniform pressure is applied to its surface. That is, the strains ϵ_y and ϵ_z are close to zero. The tactile sensor measures an applied pressure by detecting the positional change in the x direction, which is given by ϵ_x. Using these conditions the resulting x strain can be computed.

First, we obtain the y and z stresses. Since the following relationships approximately hold

$$\begin{aligned} \epsilon_y &= \frac{1}{E}\left(\sigma_y - \tfrac{1}{2}(\sigma_z + \sigma_x)\right) = 0 \\ \epsilon_z &= \frac{1}{E}\left(\sigma_z - \tfrac{1}{2}(\sigma_y + \sigma_x)\right) = 0 \end{aligned} \tag{3}$$

which gives us

$$\begin{aligned} \sigma_y &= \tfrac{1}{2}(\sigma_z + \sigma_x) \\ \sigma_z &= \tfrac{1}{2}(\sigma_y + \sigma_x) \end{aligned} \tag{4}$$

and finally

$$\sigma_x = \sigma_y = \sigma_z. \tag{5}$$

From this we see that

$$\epsilon_x = \frac{1}{E}\left(\sigma_x - \frac{1}{2}(\sigma_x + \sigma_x)\right) = 0. \tag{6}$$

This result indicates that the tactile sensor would not detect the applied pressure at all, since no positional change is induced in

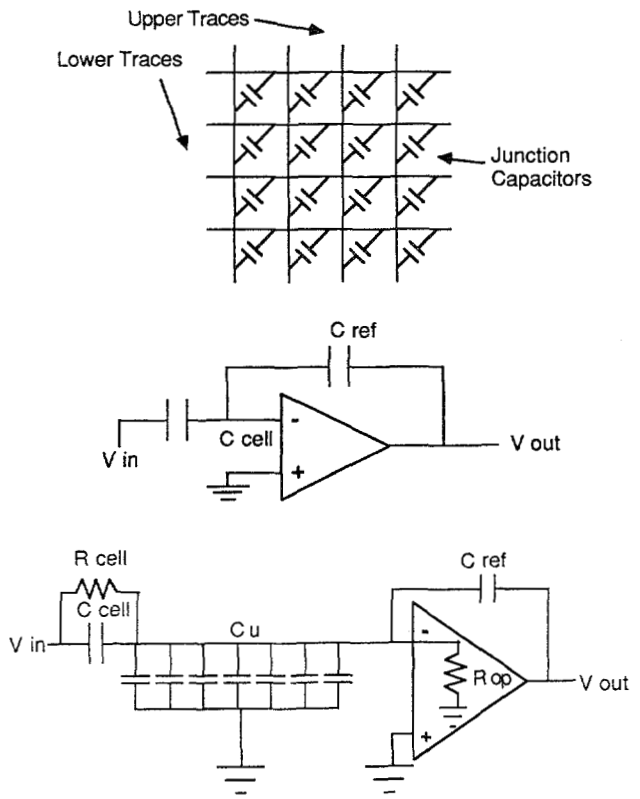

Figure 1: *Capacitance array schematic diagrams.*

the z axis. In essence, there is no "escape" path for the rubber to take to relieve the applied pressure. The applied pressure is just converted into internal stresses.

Even if we relax the uniform pressure to the yz surface assumption, using a flat sheet of rubber causes problems. If a point pressure source is applied to its surface, complex positional changes in the z direction will result, making it difficult to infer the actual contact profile. For example, material around the contact area will bulge out of the sensor's surface.

To overcome this problem, we have formed the elastic-dielectric layer into a sheet with protruding round tabs. As pressure is applied to its top, the tabs compress, and the material expands to fill the surrounding air gaps. In essence, the tabs permit the material to expand in the y and z directions and allow compression in the x direction.

Now there will be no stress in the yz plane, since it is all transformed into strain. This allows computation of the positional change in the x axis that the previous stimulus will induce:

$$\epsilon_x = \frac{1}{E}(\sigma_x + 0) = \frac{1}{E}\sigma_x. \tag{7}$$

This indicates that the tactile sensor equipped with rubber tabs can detect the applied pressure.

Phillips and Johnson [1981] discuss the mechanoreceptors in the human finger. They found that a *plane stress* assumption best fits experimental receptor response data. A plane stress model indicates that all stress is confined to the xy plane of the skin. Escape occurs along the z axis. Adding rubber tabs to the tactile sensor makes it more closely approximate the human skin, in this respect.

In addition, the pressure sensitivity of the device is controlled by the properties of the elastic-dielectric material. The stiffness of the rubber, along with the height of the protruding tabs, play a role in the overall sensitivity and the pressure ranges that can be obtained.

Recall the basic design of the sensor. Its upper layer contains rows of parallel conductors, placed perpendicular to a lower layer of parallel conductors. The two layers are separated by the elastic-dielectric material. At each intersection of an upper trace and a lower trace, a capacitor is formed. The overall interconnection pattern results in the schematic diagram shown in Figure 1.

This interconnection pattern constrains the schemes available for detecting each cell's capacitance. One can readily see that each small capacitor cannot be connected to a detector alone. In fact, the best that can be done is to select the row line and column line corresponding to the cell. The other cells connected to the selected row and column will affect the output value. The detection electronics must minimize the effects of these other cells. In effect, the detection electronics must isolate each cell in the array from all others, when taking its reading.

An amplitude modulation detection method is used for measuring the capacitance of each cell in the array, as shown in Figure 1. Unlike schemes that utilized a fixed voltage on a cell, amplitude modulation overcomes the effects of leaky capacitors. The cells formed by the upper and lower plates of the sensor will lose a relatively large amount of charge between them. By time varying the voltage on the plates, however, the charge losses will be averaged out of the voltage measurement. The relationship between charge and voltage for a capacitor is given by,

$$Q = CV, \tag{8}$$

where Q is the plate charge, C is the capacitance, and V is the voltage between the plates. The input signal V_{in} is varied over time. If we assume C is fixed, and that V varies over time, differentiating Equation 8 gives

$$i = \frac{dC}{dt} = C\frac{dV}{dt}. \tag{9}$$

The current flow i varies continuously, since the input signal is not constant. Since the junction charge is constantly changing, it is much less sensitive to capacitance leakage than with other measurement schemes. So, if $V_{in} = \sin\omega t$, the circuit output is given by:

$$V_{out} = -V_{in}\frac{C_{cell}}{C_{ref}}, \tag{10}$$

where C_{ref} is the feedback capacitor selected to give an appropriate gain.

Equation 10 shows that the output of the amplifier is just a modulated version of the input signal. To measure the capacitance of C_{cell}, the variation in amplitude of the sinusoidal output waveform is detected. First, the output waveform is precision rectified. In essence, its absolute value is obtained. Next, additional gain is applied, and low pass filtering converts the time varying waveform to a direct current signal with magnitude proportional to the root mean square voltage of the original signal. Conveniently, root mean square detector chips can be used to perform most of the detection electronics, greatly reducing the circuit's complexity.

To better understand the sensor's performance, and to select the operating frequency for the input waveform, a more detailed analysis is needed. The frequency of the input signal governs the reactance (generalized resistance) of a capacitor, which is given by:

$$\mathbf{Z} = \frac{1}{j\omega C}, \tag{11}$$

where ω is the input signal frequency. From this equation we see that the higher the input frequency, the less reactance the capacitor has, and the greater the current flow through it. Since C_{cell} is on the order of 1.0 pf, a relatively high frequency is needed to obtain even a small current. Assuming an operation frequency of 100K hertz, the capacitor has a generalized resistance of 10 megaohms. Since the operational amplifier input resistance should be large relative to this, an FET input device

and a high frequency signal should be used.

The preceding assumption of infinite operational amplifier gain must be relaxed to fully understand the performance of this detection scheme. Since an amplifier has a finite gain-bandwidth product, high frequency input signals will result in significantly lower amplification. If this is the case, Equation 10 will no longer hold.

The input signal frequency cannot be increased at will. It will eventually deteriorate the amplifier's performance. On the other hand, the input frequency cannot be too low, or not enough current will flow though the input capacitor. To fully understand this tradeoff, however, we must consider the entire sensor in our model.

The effective schematic of the capacitive array is show in Figure 1. A scan of the array should measure the capacitance of each of these cells. The scanning electronics must read each cell individually, and must overcome the cross-talk that the interconnect pattern might cause. To do this, an amplifier is connected to each of the sensor's rows, while an input signal is applied to one column at a time, in a sequential fashion. Hopefully, the row amplifier outputs will correspond to the capacitance of the selected column's cells.

Figure also shows 1 a more detailed model of the sensor's electronics. Here, the 7 capacitive cells in the column that are not selected are shown connected to the amplifier's negative input, and are labeled C_u. The amplifier's negative input is modeled as a resistor to ground, to indicate that some current flows into it. The resistor R_{cell} models the sensed capacitor's leakage. Applying Kirchhoff's's current law to the junction at the amplifier's negative input gives:

$$\frac{\frac{V_{out}}{G} - V_{in}}{\mathbf{Z}_{cell}} + \frac{\frac{V_{out}}{G}}{\mathbf{Z}_u} + \frac{\frac{V_{out}}{G}}{\mathbf{Z}_{op}} + \frac{\frac{V_{out}}{G} - V_{out}}{\mathbf{Z}_{ref}} = 0, \qquad (12)$$

where G is the gain of the amplifier at the particular operating frequency, $\mathbf{Z}_u$ is the effective impedance of the parallel combination of the other capacitors on the selected column, $\mathbf{Z}_{op}$ is the impedance of the amplifier's negative input, and $\mathbf{Z}_{cell}$ is the impedance of the sensed capacitor and its plate leakage. The impedances are given by:

$$\begin{aligned} \mathbf{Z}_{cell} &= R_{cell}/(j\omega R_{cell}C_{cell} + 1) \\ \mathbf{Z}_u &= R_u \\ \mathbf{Z}_{op} &= R_{op} \\ \mathbf{Z}_{ref} &= 1/j\omega C_{ref}. \end{aligned} \qquad (13)$$

Solving for V_{out} gives

$$V_{out} = -V_{in}GR_{op} \cdot \frac{j\omega C_{cell}R_{cell} + 1}{j\omega R_{cell}R_{op}(C_{ref}G + C_u - C_{ref} + C_{cell}) + R_{op} + R_{cell}}. \qquad (14)$$

Since FET input amplifier are used, we can assume R_{op} is very large:

$$V_{out} = -V_{in}G\frac{C_{cell}R_{cell} + 1}{j\omega R_{cell}(C_{ref}G + C_u - C_{ref} + C_{cell}) + 1}. \qquad (15)$$

Under ideal conditions, where both G and R_{cell} are very large, Equation 15 gives the desired result:

$$V_{out} = -V_{in}\frac{C_{cell}}{C_{ref}}. \qquad (16)$$

The effects of plate leakage can be examined using Equation 15. For large gain G, the magnitude of V_{out} is

$$V_{out} = V_{in}\sqrt{\frac{1}{C_{ref}^2 R_{cell}^2 \omega^2} + \frac{C_{cell}^2}{C_{ref}^2}}. \qquad (17)$$

Errors in the output signal occur when R_{cell} is large or ω is small. Hence choosing a large value for ω minimizes leakage affects.

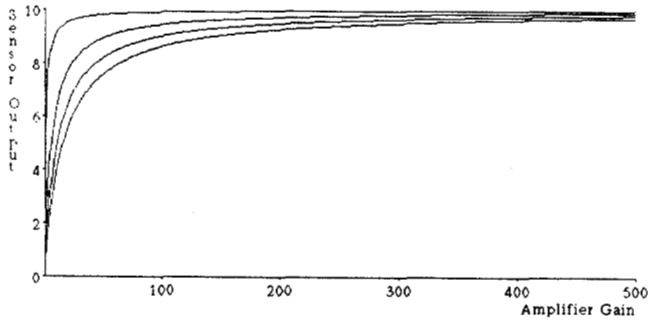

Figure 2: *Graph of the Tactile Sensor's Crosstalk Immunity with respect to amplifier gain. C_u ranges from 0 pf to 20 pf.*

If we assume the drive frequency is high enough to ensure low plate leakage, Equation 15 gives us

$$V_{out} = -V_{in}\frac{C_{cell}G}{C_{ref}G + C_u - C_{ref} + C_{cell}}. \qquad (18)$$

Ideally, V_{out} should be independent of the capacitors that are not selected (C_u). If we assume that C_{cell} has a capacitance of 1.0 pf, and C_{ref} has a capacitance of 1.0 pf, and V_{in} has amplitude 10, V_{out} should be 10. Any variation from this value will result in an erroneous measurement of the cell's capacitance. Equation 18 can be used to determine the gain required for this to be the case.

The graph in Figure 2 shows the effects of G and C_u on sensor output, as obtained from Equation 18. Sensor output is plotted against increasing gain. Ideally, the output should be 10, and any deviation from that line is undesirable. Several curves are plotted for different values of C_u, since its actual value depends on the force distribution on the sensor pad. The graph indicates that for gain over approximately 200, adequate performance is obtained. This limits the operating frequency of the input signal to the gain-bandwidth product of the amplifier divided by 200. Using this criterion, a driving signal of 200K hertz was selected for the prototype sensor.

Fabrication of the Capacitive Based Contact Sensor

The dielectric is constructed so each capacitor in the sensor array has a tab between it. Since the dielectric constant of air is lower than that of rubber, it is best to place the tabs at the capacitor junction sites. The current dielectric has a 0.25 mm thick backing with the tabs protruding out from 0.25 mm to 0.75 mm, depending on the desired force range. The tab diameter is 1.4 mm. Experimental results determined that these values gave suitable performance for an overall device sensitivity in the 0 to 200 grams per square millimeter range.

To form an array of capacitors, electrical traces are attached to the dielectric's upper and lower surfaces, with the upper traces placed perpendicular to the lower ones. A capacitor is formed at each of the trace intersections. A thin layer of electrically insulating silicone rubber is placed around the device to provide electrical shielding. Finally, the sensor is covered with conductive silicone rubber to reduce external electrical interference. Figure 3 diagrams a cross section of the device.

The current prototype has 8 upper conductive traces and 8 lower conductive traces, forming 64 force sensitive capacitive cells. The scanning electronics read force values off the array by detecting each cell's capacitance.

The traces are made of an electrically conductive silicone rubber that bonds to the dielectric layer. The parallel trace pattern is silk screened onto the dielectric layer. The lower dielectric surface must first be made into a flat surface suitable for the traces. To do this, a thin sheet of electrically insulating

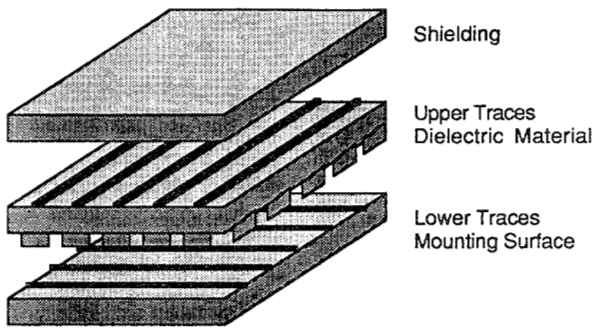

Figure 3: *Tactile sensor cross section. From top to bottom: upper conductive traces, elastic-dielectric material, lower conductive traces. The entire unit is covered with electrical shielding.*

silicone rubber is bonded to the bottom of the protruding tabs. The lower conductive traces are bonded onto this surface. Currently the traces are 1.27 mm wide, with 0.63 mm gap between adjacent rows. Hence, the capacitor plate area is 1.27 square mm, and the center-to-center cell separation is 1.9 mm.

The sensor must be shielded from stray electrical interference. Without proper shielding, the small capacitances that are to be detected at the trace junctions would be swamped by parasitic affects. To do this, the sensor package is covered with an electrically conductive material. Before this can be done, however, the upper and lower traces must be covered with an thin insulating rubber layer, and wires connected to the traces must be brought out from the package.

The scanning electronics utilize the amplitude modulation scheme previously discussed. An amplitude detector is connected to each column conductor. The drive signal is applied to each row sequentially, with the other rows grounded. The entire array is scanned by applying the drive signal to each row while reading the column amplifier outputs.

Performance Results

A series of experiments was performed to quantify the tactile sensor's performance. The set of experiments selected identify such criteria as pressure sensitivity, shape discrimination, repeatability, stability, and hysteresis.

To gather more accurate and complete data, a tactile sensor tester was developed. The device can apply a force accurately at any point on a tactile sensor pad. A stepper motor controlled *xy* positioning table moves the pad, and a stepper motor controlled linear slide mounted perpendicular to the table applies the force. The three motors are under complete computer control. If a probe tip were mounted directly on the *z* axis, a small position change would produce a large force increase into the sensor since the slide advances a relatively large distance per step. In effect, the granularity of forces that could be applied would not be adequate. To overcome this, a small linear slide is mounted onto the tester's *z* axis and the probe is attached to the outer side of the slide. A spring is connected between the *z* axis and the top of the probe. As the probe is pressed into the sensor pad, the spring compresses, and the applied force increases. The linear slide keeps the position of the probe aligned with the axis. To accurately measure the force being applied, the probe tip is mounted onto a load cell. The load cell's force output is sent to an analog to digital converter for computer processing. The experiments described in the following sections were conducted using this device.

Pressure Sensitivity

One of the most important performance criterion to establish is the sensor's pressure sensitivity. In general, the sensor's response is affected by the applied force *and* the force distribution. Unfortunately, the response per force unit area is not invariant over the applied area. That is, as the area of an applied stimulus of constant pressure is changed, the sensor's output also changes.

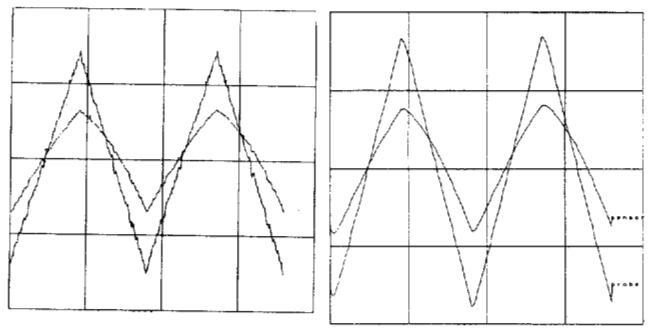

Figure 4: *Left: raw output of probe; applied force overlayed with the sensor output. Right: low passed filtered output of probe; applied force overlayed with sensor output.*

The response variation due to stimulus size is due to both mechanical and electrical properties. If the sensor were composed of discrete force sensing elements that have no connection to each other there would be no sizing affect. However, since most sensors have interconnecting components in them (an elastomeric covering, for example), the mechanical connections become a factor. The sensor's scanning electronics also play a role in its response. Hopefully the electronics can read a cell without ambiguity. In some sensors, however, the values of neighboring cells can have effects on each other.

Figure 4 shows the raw data from the probe overlayed on the raw data from one tactile cell of the sensor. The probe pressure is increased and decreased at a linear rate of approximately 1 Hertz. The cell shows good linear response during these trials. The bottom plot in Figure 4 shows the same data low-pass filtered to eliminate noise generated by the testing apparatus.

Hysteresis is often cited as a problem with elastomeric based devices such as the capacitive array. We did not experience noticeable hysteresis in the classical notion. Instead, a droop and sag related to the elastomeric properties of the material was present [Fearing 1986]. In essence, the rubber dielectric expands at a slower rate than it contracts, when subjected to the same force. Hysteresis implies that the sensor would never return to its relaxed state, as absolute energy is lost from the system. We did not experience this behavior in our experiments. None the less, the droop and sag is a problem if the sensor is being used to accurately measure an applied force. In principle this could be modeled using a damped spring system; however, the noise present in our data made such corrections difficult.

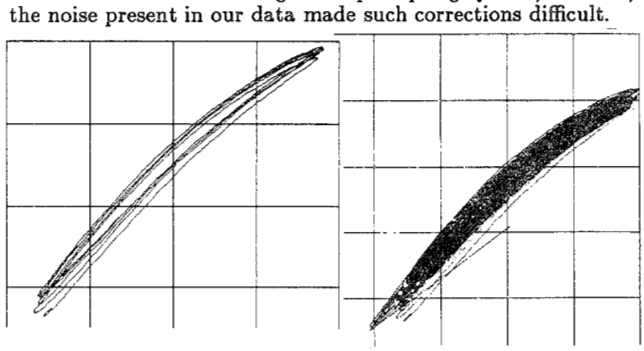

Figure 5: *Left: difference in loading and unloading the sensor over four samples. Right: difference in loading and unloading the sensor over many trials.*

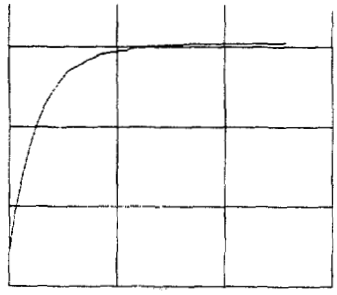

Figure 6: *Displacement of the sensor for a constant force over time.*

To examine this phenomenon two separate experiments were performed. In the first, a probe was pushed into the center of one cell. The sensor's output was sampled while the force was varied from 0 to 150 grams, and then back to 0 grams. The data from this experiment is shown in Figure 5. This data is shown by plotting the force of the probe verses the sensor output. A difference in loading and unloading the sensor is readily observed. The bottom figure shows, however, that this difference lies within the noise range of the system.

In the second experiment, the probe was pressed into the sensor at a constant force and the sensor was then read over a period of time. Figure 6 shows the sensor output verses time. The sag is apparent in this data.

In actuality, "hysteresis" in tactile sensors may not prove to be as major problem as some researchers have suggested. Human skin displays substantial hysteresis, yet our tactile sensing ability is well equipped to handle complex manipulatory tasks. In addition, a robotic system can compensate for their response variability by recording the time history of the manipulator motion. Since the robot knows if its motion is causing increasing or decreasing force into an object, it can select the appropriate half of the hysteresis curve to translate sensor output into force. Even more importantly, this problem is unavoidable since tactile sensors must have elastomeric coverings.

Measurement Repeatability

Tests were performed to determine how accurately a sensor can measure an applied force. The tester probe was poked into a capacitive cell a number of times, and the sensor's output was recorded. In each sample, sensor output that corresponds to a particular probe force was plotted. The data in Figure 7 shows that there is considerable noise in the system, from sample to sample. Figure 5 showed, however, that variability within each trial is minimal. Thus the sensor is currently very good at detecting *changes* in the applied pressure, but much poorer at detecting absolute values of pressures.

Spatial Selectivity

The spatial resolution of the sensor is a function of the spacing between capacitive cell centers and the elastomeric properties of the dielectric and protective coverings. For a sensor that records just surface normal force, a point source should only be detected by the one or more cells directly in contact with the stimuli; spreading or blurring to adjacent cells should be minimal. Obviously, having a sharp sensor response will give more detail in tactile force outlines of probed objects. In some cases, however, it may be useful to propagate strains between adjacent sensor sites. Fearing and Hollerbach [1984] theoretically show how strain sensors placed below a surface can extract the angle of inclination, location, and magnitude of a load line.

To measure the spatial selectivity of the sensor pad the tactile tester was programmed to step linearly across the sensor pad and to apply a uniform force at each location. The probe was advanced at 0.1 mm intervals and applied 100 grams force

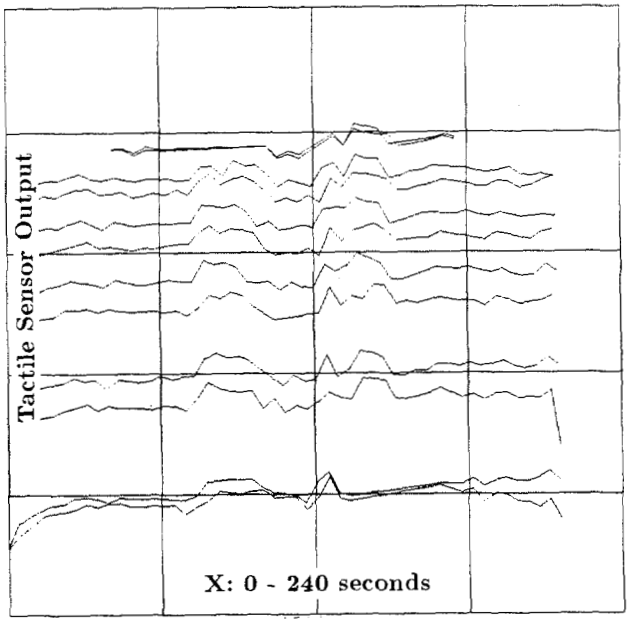

Figure 7: *Displacement of the sensor over several samples for several forces. The variability over different samples is apparent.*

at each point. One would expect that a cell would respond best to a force applied directly at its center. As the probe moves further away, a drop in output should be noticed. The receptive field of each cell is affected mostly by the mechanical properties of the rubber elastic-dielectric layer with the tabs helping to localize a cell's response.

The plots shown in Figure 8 summarize the results of this test. The curves show the response of 3 adjacent sensor cells as a probe is linearly stepped across them. The peaks of the plots are spaced approximately 2 mm apart as expected, since this is the array's center-to-center spacing. Notice that there is some response overlap between adjacent cells. That is, when probing on a cell, the neighboring cell will show some response as well. This behavior is desirable since it avoids the dead zones between cells that would otherwise result.

Shape Discrimination

The shape of an object can be obtained by pressing the tactile sensor against it, and recording the resultant force profile. In cases where visual inspection is impossible, such as when a manipulator end-effector obscures the view, this is especially desirable. The spatial resolution results of the previous section indicate that the sensor's shape discrimination ability should be good. To verify this, small objects were pressed against the tactile pad, and the force outputs were recorded.

Since shape recognition utilizes all 64 tactile cells, a calibration procedure must be employed to normalize the array's response. That is, each cell should read the same value when equal forces are applied to them. Variations in cell output with an applied force occur for several reasons. A cell's force response is related to the compressibility of the elastic-dielectric material at its location. Small variations in the silicone rubber's properties cause differences in compressibility at different pad locations. In addition, the scanning electronics themselves have small component variations, inducing differences in the force output of the cells.

To calibrate the sensor the tactile tester apparatus was employed. The tester was programmed to probe at the center of each tactile cell with a number of different forces. The actual

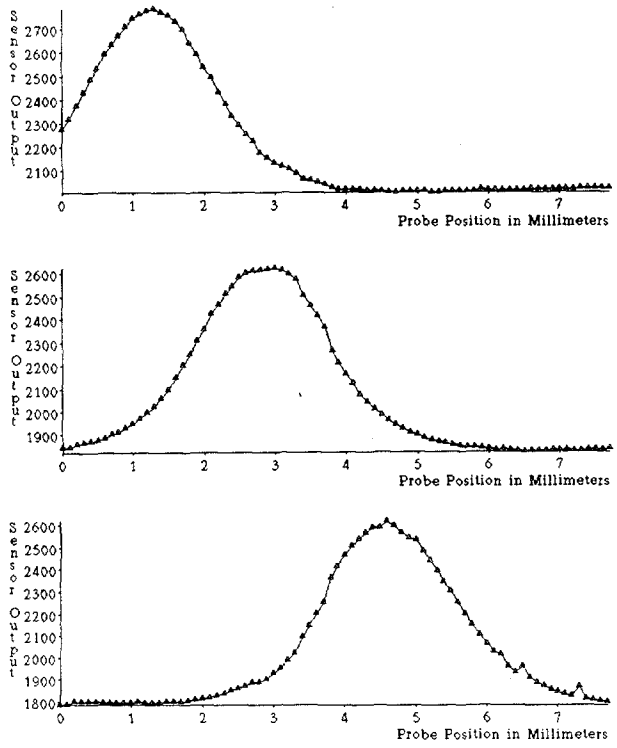

Figure 8: *Tactile Spatial Selectivity. Response of sensor cells as a probe is applied to the pad at 0.1 mm linear spaced intervals. The curves, from top to bottom, show the response of the 3 adjacent cells.*

applied force and the cell's output were recorded for each measurement. A least squares procedure was used to fit a straight line to these data points. Since a preceding section showed that the sensor's force response is linear, fitting the data points to a straight line is considered adequate. The actual force output is obtained from a sensor's cell output from

$$\frac{c_{out} - b}{m} = f_{out}, \tag{19}$$

where m is the curve's slope, b is the zero force intercept, c_{out} is the raw sensor output, and f_{out} is the normalized force. Results show that the values in each sensor column are relatively constant. This occurs because each column has its own amplification electronics. Evidently the variations in the amplifier's electronic components contribute heavily to the calibration difference in force output.

Figures 9 through 13 show tactile force images. The data is displayed using three dimensional bar plots. The height of each of the 8×8 bars corresponds to the cell's force output. Figure 9 show a force image of straight edges pushed into the sensor pad. Figures 10 show an image of an integrated circuit socket. Figure 11 shows an image of a fairly complex part with two parallel edges, one thicker than the other. The actual gap between the edges is approximately 3 mm, corresponding to the 1 pixel gap shown in the image (sensor cells are spaced 1.9 mm center-to-center). Figure 12 show images of a bolt and a washer. Finally, Figure 13 shows the profile of a 6 pin molex connector. In all cases the variations in pixel height along an object's edges come from variations in the pressure distribution as the object was pushed into the sensor pad. No special provisions were taken to insure that a uniform pressure was being applied over the part.

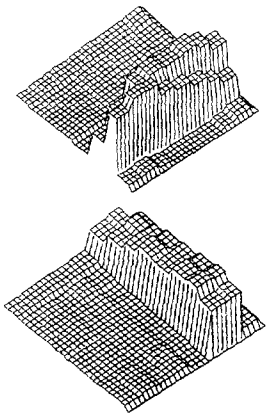

Figure 9: *Tactile images of edges. Top: aligned slightly off horizontal axis. Bottom: aligned directly on vertical axis.*

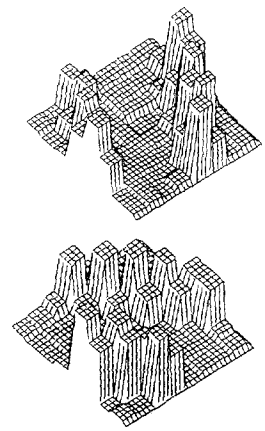

Figure 10: *Tactile images of integrated circuit socket. Top: aligned on diagonal axis. Bottom: aligned on opposite diagonal axis.*

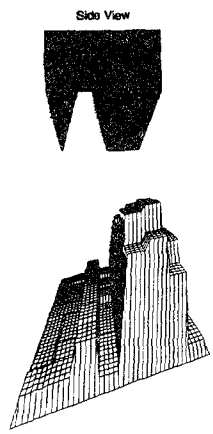

Figure 11: *Tactile image of part with two edges. Top: diagram of part. Bottom: side view image of part.*

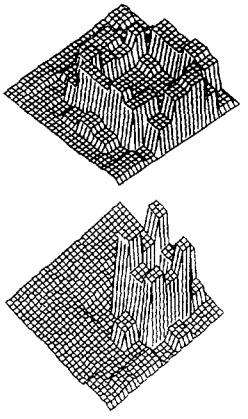

Figure 12: *Tactile images of bolt and washer. Top: bolt. Bottom: washer.*

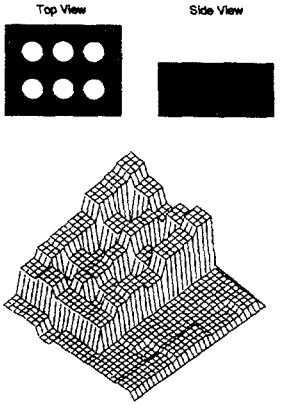

Figure 13: *Tactile image of a Molex connector. Top: diagram of connector. Bottom: tactile image.*

Discussion

This paper examined a tactile sensor with an 8×8 array of capacitive cells. Before the sensor's design was specifically discussed, several questions concerning a contact sensor design were posed. The questions were used to formulate a general sensor design methodology. The questions, together with the description of the tactile sensor prototype, attempted to give the reader a framework for designing contact sensors for other robotics applications.

Acknowledgments

We are deeply indebted for John Hollerbach and Sundar Narasimhan's invaluable assistance. In addition, Amicon Corporation helped develop the silicone rubber materials used in the sensor.

This report describes research done at the Artificial Intelligence Laboratory of the Massachusetts Institute of Technology. Support for the laboratory's artificial intelligence research is provided in part by the System Development Foundation, in part by the Office of Naval Research under contract N00014-81-0494, and in part by the Advanced Research Project Agency under Office of Naval Research contracts N00014-80-C-050 and N00014-82-K-0334. Support for the author was provided in part by a National Science Foundation fellowship.

References

1. **Binford, T. O.,** "Sensor Systems for Manipulators," *Proc. of Conference on Remotely Manned Systems,* Cal Tech, pp. 283-291, 1972.

2. **Boie, R. A.,** "Capacitive Impedance Readout Tactile Image Sensor," *Proc. IEEE International Conference on Robotics and Automation,* pp. 370-379, Atlanta, 1984.

3. **Brockett, R. W.,** "Robot Hands with Rheological Surfaces," *Proc. IEEE International Conference on Robotics and Automation,* pp. 942-947, St. Louis, 1985.

4. **Chomerics Corporation,** "EMI Shielding Engineering Handbook," Woburn, MA, 1985.

5. **Chun, K. J., Wise, K. D.,** "A Capacitive Silicon Tactile Imaging Array," *Proc. IEEE International Conference on Solid-State Sensors and Actuators,* pp. 22-25, Philadelphia, 1985.

6. **Dario, P., De Rossi, D.,** "Tactile Sensors and the Gripping Challenge," *IEEE Spectrum,* vol. 22, no. 8, August 1985.

7. **Fearing, R. S., Hollerbach, J. M.,** "Basic Solid Mechanics for Tactile Sensing," *Proc. IEEE International Conference on Robotics and Automation,* pp. 266-275, Atlanta, 1984.

8. **Fearing, R. S., Rise, A., Binford, T. O.** "A Tactile Sensing Finger Tip for a Dextrous Hand," *Proc. of SPIE Conference on Intelligent Robots and Computer Vision,* Cambridge, MA, Oct.1986

9. **Grimson, W. E. L., Lozano-Perez, T.,** "Model-Based Recognition and Localization from Tactile Data," *Proc. IEEE International Conference on Robotics and Automation,* Atlanta, pp. 248-255, 1984.

10. **Harmon, L. D.,** "Automated Tactile Sensing," *The International Journal of Robotics Research,* vol. 1, no. 2, pp. 3-32, 1982.

11. **Hollerbach, J. M.,** "Tactile Sensors and Interpretation of Contact Features," *Proceedings of the NSF Workshop on Intelligent Robots: Issues and Achievements,* SRI International, Menlo Park, CA, Nov. 13-14, 1984.

12. **Jacobsen, S. C., Wood, J. E., Knutti, D. F., Biggers, K. B.,** "The Utah-MIT Dextrous Hand: Work in Progress," *The International Journal of Robotics Research,* vol. 3, no. 4, pp. 21-50, 1984.

13. **Lederman, S., Klatzky, R.,** "Hand Movements: A Window into Haptic Object Recognition," *Proc. of the 26th Annual Meeting of the Psychonomic Society,* Boston, 1985.

14. **Ogorek, M.,** "Tactile Sensors," *Manufacturing Engineering,* vol. 94 no. 2, pp. 69-77, 1985.

15. **Phillips, J. R., Johnson, K. O.,** "Tactile Spatial Resolution. III. A Continuum Mechanics Model of Skin Predicting Mechanoreceptor Responses to Bars, Edges, and Gratings," *Journal Of Neurophysiology,* vol. 46, no. 6, pp. 1204-1225, Dec. 1981.

16. **Siegel, D. M., Garabieta, I., Hollerbach,** J. M., "A Capactive Based Tactile Sensor," *Proc. of SPIE Conference on Intelligent Robots and Computer Vision,* Cambridge, MA, pp. 153-161, Sept. 1985.

17. **Siegel, D. M.,** "Contact Sensors for Dexterous Robotic Hands," *MIT AI Laboratory Technical Report No. 900,* Cambridge, MA, Aug. 1986.

18. **Timoshenko, S., Goodier, J. N.,** "Theory of Elasticity", McGraw-Hill, 1951.